



Hybrid torque modeling of spherical actuators with cylindrical-shaped magnet poles

Liang Yan^{a,*}, I-Ming Chen^b, Chee Kian Lim^b, Guilin Yang^c, Wei Lin^c, Kok-Meng Lee^d

^aSchool of Automation Science and Electrical Engineering, Beihang University, Beijing 100191, China

^bSchool of Mechanical and Aerospace Engineering, Nanyang Technological University, Singapore 639798, Singapore

^cMechatronics Group, Singapore Institute of Manufacturing Technology, 71 Nanyang Drive, Singapore 638075, Singapore

^dGeorge W. Woodruff School of Mechanical Engineering, Georgia Institute of Technology, Atlanta, GA 30332-0405, USA

ARTICLE INFO

Article history:

Received 27 December 2009

Accepted 25 August 2010

Keywords:

Torque modeling
Spherical actuator

ABSTRACT

A ball-joint-like three-degree-of-freedom (3-DOF) spherical actuator which features a ball-shaped rotor with multiple permanent magnet (PM) poles and a spherical-shell-like stator with air-core coils is proposed to achieve omni-directional smooth motion in only one joint. Unlike previous study in which dihedral-shaped PMs are employed as the rotor poles, this paper utilizes cylindrical-shaped PMs to facilitate the fabrication and reduce the system cost significantly. Torque output of the spherical actuator is formulated with a hybrid method, i.e., using both analytical and experimental methodologies. Specifically, the analytical torque model of spherical actuator with dihedral-shaped PM poles is derived. Then a research prototype with cylindrical-shaped PM poles is developed, and a torque measurement testbed is built up to conduct experiment on the prototype. As the torque variation trend of actuators using two different types of PM poles with respect to the rotor orientation is similar, parameters in the analytical model are adjusted to fit with the experimental measurements. The resulting torque model can be employed for real-time motion control of the actuator. The cylindrical-shaped PM poles also reduce the inertial moment of the rotor by 60%, which is favorable for achieving better dynamic performance of the spherical actuator.

© 2010 Elsevier Ltd. All rights reserved.

1. Introduction

Single-axis actuators based on various principles [1–4] have been developed for long history. Several single-axis actuators can be connected in parallel or in series to achieve multi-degree-of-freedom (multi-DOF) rotational motions. This type of mechanism has disadvantages of bulky structure, large inertia moment and singularity existence in workspace. To eliminate these drawbacks, spherical actuators that can generate multi-DOF rotational motion in only one joint have been proposed by researchers. The first 2-DOF spherical induction motor has been designed by Laithwaite and Williams [5,6]. Torque model of this induction motor was derived by integrating the Maxwell stress moment over the spherical rotor surface [7]. A spherical stepper [8,9] and a spherical wheel motor [10–12] have been developed by Lee et al. based on the principle of variable reluctance (VR). The torque output of these motors was formulated by using co-energy method, which shows that the actuator torque depends on the current inputs and the magnetic reluctance at air gaps [13]. Spherical actuators that can achieve 2/3-DOF motions have been developed by Wang et al.

[14–16]. The torque output was formulated with Lorentz force law analytically. Chirikjian et al. [17] made a spherical stepper with a PM-pole rotor and a stator with an array of coils. Difference in the symmetric layout of rotor and stator poles allows stepping motion in three orientations. Yang et al. [18] have proposed a 3-DOF spherical actuator in which the rotor can make an arbitrary orientation and a spin by interactions among rotor and stator poles. The torque output was formulated with Coulomb's law. Kahlen et al. [19] have developed a spherical motor consisting of a rotor with 112 PM poles and a stator with 96 windings. The poles were arranged symmetrically corresponding to longitude and latitude of a globe. The torque was calculated numerically. Dehez et al. [20] developed a 2-DOF spherical induction motor with various rotor and stator structures. Its performance in terms of characteristic torque-speed and efficiency has been analyzed with Maxwell tensor.

In our previous study [21], a 3-DOF spherical actuator consisting of a PM-pole rotor and a stator with two layers of coils has been developed. The rotor and stator are parameterized, and generic method based on Lorentz force law was employed to formulate torque output of the actuator analytically. The proposed structure configuration allows more rotor and stator poles to be incorporated and thus to increase the working range as well as motion resolution of the actuator. However, the use of dihedral-shaped PM poles complicates the magnet fabrication and increases the system cost greatly. Therefore, in this study, cylindrical-shaped

* Corresponding author.

E-mail addresses: yanliang@pmail.ntu.edu.sg (L. Yan), michen@ntu.edu.sg (I-Ming Chen), cklim@ntu.edu.sg (C.K. Lim), glyang@simtech.a-star.edu.sg (G. Yang), wlin@simtech.a-star.edu.sg (W. Lin), kokmeng.lee@me.gatech.edu (K.-M. Lee).

PM poles that are widely available in the market are proposed as the rotor poles. The employment of cylindrical-shaped PM poles reduces the inertial moment of the rotor by more than 60%, which can improve dynamic response of the rotor greatly. The torque output of this spherical actuator is formulated with a hybrid method. Specifically, the analytical torque model of a 3-DOF spherical actuator with dihedral-shaped magnet poles is presented. A research prototype of the spherical actuator with cylindrical-shaped PM poles is developed, and an experimental testbed is built up to conduct the torque measurements on the prototype. As the actuator torque variation with respect to rotor orientations for both PM-pole designs is similar, parameters in the analytical model are adjusted to fit with the experimental results. The obtained torque model could thus be utilized to analyze the system output performance, and to facilitate real-time motion control of the actuator.

2. Concept design and pole configuration

2.1. Selection of PM and coil pairs

As shown in Fig. 1, there are various combinations of rotor and stator pole configuration. The configuration of PM with the air-core coil has the advantage of linear relationship between torque output and current input. This feature benefits the real-time motion control of the spherical actuator. Compared with iron-core coil, the torque generated by air-core coils may be lower as magnetic flux leakage is relatively high. However, iron stator can be employed to reduce the magnetic energy loss, and thus to increase the force to power ratio. The effect of iron stator on actuator torque will be studied in another work. In addition, for PM actuators, no electrical energy is absorbed by the field excitation system. Thus, there is no excitation loss. This indicates that the efficiency of PM actuator can be higher than that of actuators using only electromagnets. In other words, high torque or output power per volume and thus better dynamic performance can possibly be achieved with PM actuators. The cost of rare-earth PM has also dropped significantly. These features urge the wide use of PMs in actuators [22–25] and its employment in our study.

The pole arrangement on actuators may be constructed in two ways. It can have either moving coils and stationary magnets or moving magnets and stationary coils. The latter type of configuration does not require a cable to the moving part [25] that may complicate the power supply and constrain the motion range of moving

parts. Therefore, the coils are mounted on the stator to facilitate the power supply and the system motion control in our spherical actuator. The structure of the proposed PM spherical actuator is illustrated in Fig. 2. PM poles are mounted on the rotor equator to generate a three-dimensional (3D) magnetic field in surrounding space. Layers of coils are assembled on the stator to interact with the magnetic field of PM poles, and thus to produce the spherical motion of the rotor in 3-DOF.

2.2. Geometry of rotor and stator poles

- (1) *PM-pole parameters*: Fig. 3 presents the shape of a single rotor pole—a dihedral cone enclosed by $ABCD$ and $abcd$. The dihedral cone is specified by four parameters: longitudinal angle α , latitudinal angle β , rotor radius R_r and rotor core radius R_b . Modeling a single pole as a dihedral cone has several benefits. Due to the 3-DOF rotational motion of the rotor, the spherical surface of the dihedral-cone-shaped pole can avoid the interference between coils and PM poles, whilst making full use of the rotor workspace. Furthermore, the volume of the rotor pole can be specified in spherical coordinates, which facilitates the formulation of the actuator torque. By varying the parameters of dihedral cone, the study of optimum magnet-pole pattern can be carried out.
- (2) *Coil parameters*: Conical-shaped coil is utilized in this PM spherical actuator as shown in Fig. 4. The sectional area of coil is specified by four parameters, i.e., R_0 – the distance

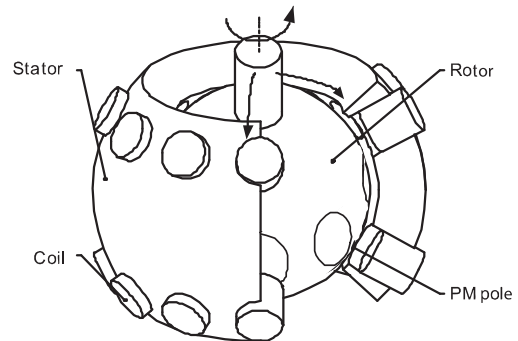


Fig. 2. Concept design of the spherical actuator.

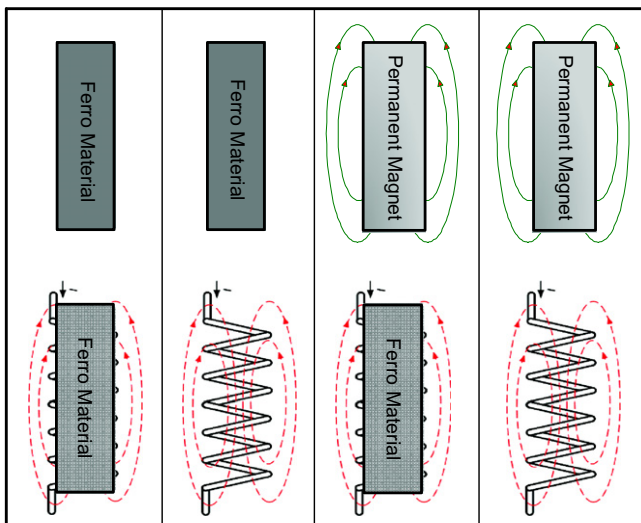


Fig. 1. Poles' configuration of the spherical actuator.

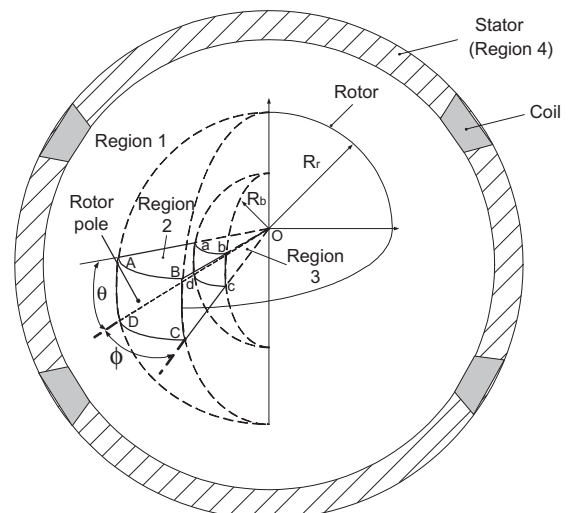


Fig. 3. Region division of rotor and stator space.

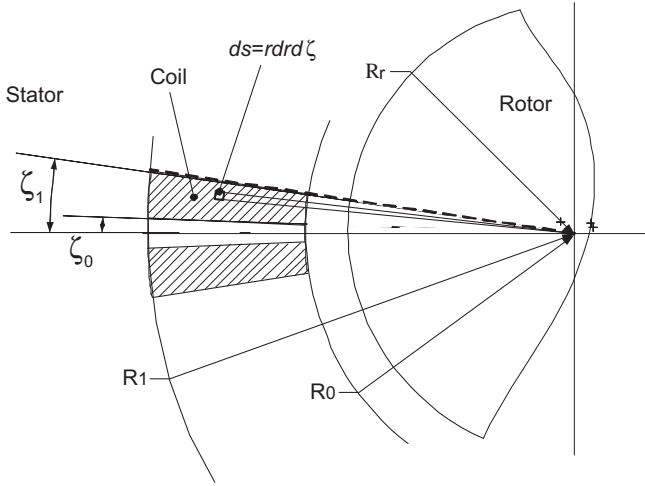


Fig. 4. Sectional view of the coil shape.

from the rotor center to the top surface of the coil, R_1 – the distance from the rotor center to the bottom surface of the coil, ζ_0 – the inner surface angle of the coil and ζ_1 – the outer surface angle of the coil. This geometric shape can take advantage of the space surrounding the rotor effectively, and facilitate the actuator torque formulation in spherical coordinates.

2.3. Analytical torque model of the spherical actuator

(1) *Magnetic field model*: The rotor space under study is divided into three regions based on their magnetic characteristics. The air space outside the rotor is denoted as Region 1. The volume enclosed by ABCD and abcd, i.e., the PM pole (filled with rare-earth magnetic material), is Region 2. The inner core filled with ferromagnetic materials is Region 3. The relationship between flux density \mathbf{B} and field intensity \mathbf{H} for these three regions is

$$\mathbf{B}_i = \begin{cases} \mu_0 \mathbf{H}_i, \\ \mu_0 \mu_m \mathbf{H}_i + \mu_0 \mathbf{M}_0, & (i = 1, 2, 3), \\ \mu_0 \mu_r \mathbf{H}_i, \end{cases} \quad (1)$$

where \mathbf{M}_0 , μ_0 , μ_m and μ_r are residual magnetization vector, permeability of free space, relative recoil permeability of PM and relative permeability of ferromagnetic materials respectively. The scalar potential Φ is governed by Laplace equations

$$\nabla^2 \Phi_i = 0, \quad (i = 1, 2, 3). \quad (2)$$

Let M_0 be the magnitude of magnetization vector \mathbf{M}_0 . The constituents M_{0r} , $M_{0\theta}$ and $M_{0\phi}$ in spherical coordinates are

$$\begin{aligned} M_{0r} &= (-1)^{p-1} M_0 \cos \left[\phi - \alpha_0 - \frac{2\pi}{P} (p-1) \right] \sin \theta, \\ M_{0\theta} &= (-1)^{p-1} M_0 \cos \left[\phi - \alpha_0 - \frac{2\pi}{P} (p-1) \right] \cos \theta, \\ M_{0\phi} &= (-1)^p M_0 \sin \left[\phi - \alpha_0 - \frac{2\pi}{P} (p-1) \right], \end{aligned} \quad (3)$$

where $p = 1, 2, \dots, P$. P is the total number of PM poles. The radial component can be expressed as an expansion of spherical harmonic functions $Y_n^m(\theta, \phi)$ as

$$M_{0r}^s(\theta, \phi) = \sum_{n=0}^{\infty} \sum_{m=-n}^n C_{nm} Y_n^m(\theta, \phi), \quad (4)$$

where C_{nm} are coefficients determined from the surface integral of the following form:

$$C_{nm} = \int_0^\pi \int_0^{2\pi} M_{0r}(\theta, \phi) Y_n^{m*}(\theta, \phi) \sin \theta d\theta d\phi,$$

and $Y_n^{m*}(\theta, \phi)$ denotes the complex conjugate of $Y_n^m(\theta, \phi)$. The boundary conditions in between the three regions are

$$\begin{aligned} B_{1r}, B_{1\theta}, B_{1\phi}|_{r \rightarrow \infty} &= 0, B_{3r}, B_{3\theta}, B_{3\phi}|_{r=0} \neq \infty, \\ B_{1r}|_{r=R_r} &= B_{2r}|_{r=R_r}, B_{2r}|_{r=R_b} = B_{3r}|_{r=R_b}, \\ H_{1\phi}|_{r=R_r} &= H_{2\phi}|_{r=R_r}, H_{1\theta}|_{r=R_r} = H_{2\theta}|_{r=R_r}, \\ H_{2\phi}|_{r=R_b} &= H_{3\phi}|_{r=R_b}, H_{2\theta}|_{r=R_b} = H_{3\theta}|_{r=R_b}. \end{aligned} \quad (5)$$

From above equations, the magnetic field is obtained as

$$\begin{aligned} B_{1r} &= \frac{15\mu_0 M_0 a c d_4}{8\pi} \sqrt{\frac{35}{2}} r^{-6} \sin^4 \theta \cos 4\phi, \\ B_{1\theta} &= \frac{12\mu_0 M_0 a c d_4}{8\pi} \sqrt{\frac{35}{2}} r^{-6} \sin^3 \theta \cos \theta \cos 4\phi, \\ B_{1\phi} &= \frac{12\mu_0 M_0 a c d_4}{8\pi} \sqrt{\frac{35}{2}} r^{-6} \sin^3 \theta \sin 4\phi, \end{aligned} \quad (6)$$

where a , c and d_4 can be calculated with

$$\begin{aligned} a \pm bi &= \int_0^{2\pi} f(\phi) e^{-im\phi} d\phi \quad (m = 4 \text{ and } m = -4), \\ c/\sqrt{\pi} &= \int_0^\pi S_n^m \sin^2 \theta [P_n^m(\cos \theta)] d\theta, \\ f(\phi) &= (-1)^{p-1} \cos \left[\phi - \frac{\pi}{4} (p-1) \right], \quad p = 1, 2, \dots, 8, \\ S_n^m &= \sqrt{\frac{2n+1}{4\pi} \frac{(n-m)!}{(n+m)!}}, \quad d_4 = -d_4^- / d_4^+, \\ d_4^- &= R_r^6 + \frac{9\mu_m R_b^6 R_r^9}{4(\mu_r - \mu_m) R_b^9 - (4\mu_r + 5\mu_m) R_r^9}, \\ d_4^+ &= 5(\mu_m - 1) + \frac{9\mu_m (4\mu_r + 5\mu_m) R_r^9}{4(\mu_r - \mu_m) R_b^9} - (4\mu_r + 5\mu_m) R_r^9. \end{aligned}$$

(2) *Torque model*: Generally there are three commonly used methods that can be employed for the calculation of electromagnetic force and torque, i.e., Maxwell stress tensor (MST), virtual work and Lorentz force law. The MST and virtual work approaches are usually used in finite element (FE) solution of force/torque computation. Most commercial electromagnetic FE software packages use the virtual work method as it is numerically more stable than the MST method. Lorentz force law is especially useful when the force/torque is generated by a current-carrying conductor laying in the magnetic field of PM. In this study, the torque produced by a single coil is obtained by Lorentz force law

$$\begin{aligned} \mathbf{T}_i &= J_i \int_{R_0}^{R_1} \int_{\zeta_0}^{\zeta_1} \left\{ \int_C \mathbf{r}_e \times [B_{1r}(r, \theta, \phi) \mathbf{e}_r \times d\mathbf{l}] \right\} r dr d\zeta \\ &= T_c \mathbf{G}(\theta_i, \phi_i) J_i, \end{aligned} \quad (7)$$

where

$$\mathbf{T}_i = [T_{ix}, T_{iy}, T_{iz}]^T,$$

$$\begin{aligned} \mathbf{G}(\theta_i, \phi_i) &= [\mathbf{g}_x(\theta_i, \phi_i), \mathbf{g}_y(\theta_i, \phi_i), \mathbf{g}_z(\theta_i, \phi_i)]^T \\ &= \mathbf{e}_{\phi_i} (-4 \sin^3 \theta_i \cos^4 \phi_i \cos \theta_i - 4 \sin^3 \theta_i \sin^4 \phi_i \cos \theta_i \\ &\quad + 24 \sin^3 \theta_i \cos^2 \phi_i \sin^2 \phi_i \cos \theta_i) - \mathbf{e}_{\theta_i} (16 \sin^3 \theta_i \\ &\quad \times \cos^3 \phi_i \sin \phi_i - 16 \sin^3 \theta_i \sin^3 \phi_i \cos \phi_i), \end{aligned}$$

$$T_c = \frac{15}{8} \sqrt{\frac{35}{2}} \mu_0 M_0 a c R_c G'_\zeta, \quad R_c = O_{4,6} R_{c,1} + O_{4,5} R_{c,2},$$

$$R_{c,1} = (R_0^{-2} - R_1^{-2})/2, \quad R_{c,2} = (R_0^2 - R_1^2)/7,$$

$$G_\zeta = G'_\zeta - \frac{3G''_\zeta}{4}, \quad G'_\zeta = 1/5 \sin^5 \zeta_1 - 1/5 \sin^5 \zeta_0,$$

$$G''_\zeta = 1/5 \cos^4 \zeta_0 \sin \zeta_0 - 1/15 \cos^2 \zeta_0 \sin \zeta_0 - 2/15 \sin \zeta_0$$

$$- 1/5 \cos^4 \zeta_1 \sin \zeta_1 + 1/15 \cos^2 \zeta_1 \sin \zeta_1 + 2/15 \sin \zeta_1.$$

The unit vectors \mathbf{e}_{ϕ_i} and \mathbf{e}_{θ_i} in spherical coordinates can be represented in terms of Cartesian coordinates as

$$\mathbf{e}_{\phi_i} = -\sin \phi_i \mathbf{e}_x + \cos \phi_i \mathbf{e}_y,$$

$$\mathbf{e}_{\theta_i} = \cos \theta_i \cos \phi_i \mathbf{e}_x + \cos \theta_i \sin \phi_i \mathbf{e}_y - \sin \theta_i \mathbf{e}_z.$$

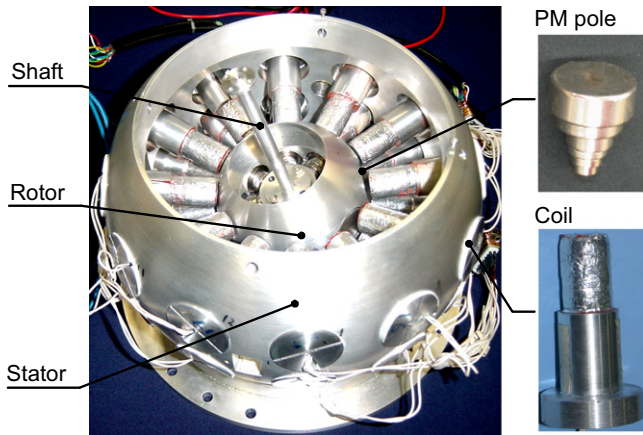


Fig. 5. Prototype of spherical actuator.

Table 1 Specifications of spherical actuator.

Inner/outer stator radius	95/112.5 mm
Rotor radius	46.5 mm
Number of rotor poles (PM)	8
Number of stator poles (coil)	24/2 layers
Number of coil turns	1027
Coil size (diameter×height)	ø25 × 30 mm
Maximum tilting angle	±11°
Maximum spinning torque	2.2 N m
Maximum tilting torque	1.2 N m

Eq. (7) represents the torque by a single coil. With N coils on the stator, the torque model of the spherical actuator with complete set of coils can be obtained

$$\mathbf{T} = T_c \mathbf{Q} \mathbf{J}, \tag{8}$$

where $\mathbf{J} = [J_1 J_2 \dots J_N]^T$ represents currents passing through N coils, and \mathbf{Q} is defined as the torque matrix

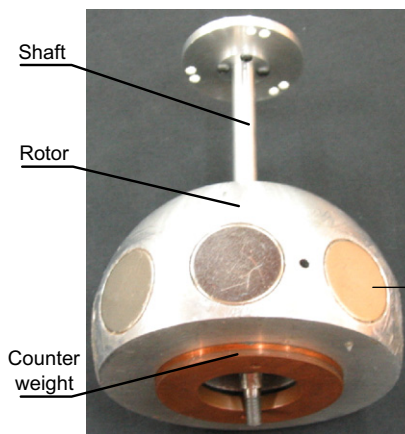
$$\mathbf{Q} = \begin{bmatrix} f_x(\theta_1, \phi_1) & f_x(\theta_2, \phi_2) & \dots & f_x(\theta_N, \phi_N) \\ f_y(\theta_1, \phi_1) & f_y(\theta_2, \phi_2) & \dots & f_y(\theta_N, \phi_N) \\ f_z(\theta_1, \phi_1) & f_z(\theta_2, \phi_2) & \dots & f_z(\theta_N, \phi_N) \end{bmatrix}.$$

3. Research prototype

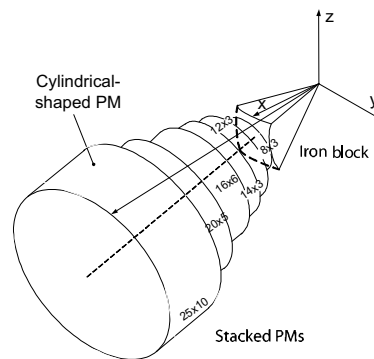
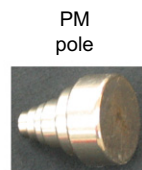
A research prototype of the spherical actuator is developed as shown in Fig. 5. One layer of eight cylindrical-shaped PM poles are mounted along the rotor equator, and two layers of air-core coils (12 per layer) are fixed on the stator symmetrically with respect to the stator equator. All coils' axes go through the rotor center. A spherical bearing is used to secure the rotor inside the stator, and adjust the concentricity of rotor and stator. The specification of this prototype is listed in Table 1. The prototype can be employed for experimental measurement on magnetic field of the rotor and actuator torque output. The stator size is much larger than that of the rotor, which facilitates the experimental works inside the stator. In the future, laminated soft iron will be used for the



Fig. 7. Testbed for force/torque measurement of single coil.



(a) PM poles on the rotor



(b) A single PM pole

Fig. 6. Utilization of cylindrical PMs for rotor poles.

construction of stator, so that the stator size can be reduced at least by half.

In the modeling study, dihedral-shaped PMs are utilized as the rotor poles, which benefits the torque modeling and actuator design optimization. However, it is complicated to fabricate and the cost is very high. Therefore, rotor poles with stacked cylindrical

PMs are proposed as an alternative design. As shown in Fig. 6, several cylindrical PMs of different sizes can be stacked together to form a rotor pole. Because cylindrical PMs are widely available in the market, the cost (only a few dollars) is ignorable compared with that of dihedral-shaped PMs (around one thousand dollars). Furthermore, by using cylindrical-shaped magnet poles, inertial moment of the rotor can be reduced by more than 60%, which is favorable for improving dynamic performance of actuator. Back iron block is mounted at the rotor center to stick PM poles together and reduce the magnetic energy loss.

Table 2
Specifications of the torque measurement apparatus.

DC power supply	Model	Topward 3303D
	Range	0–30 V, 0–3 A
Torque sensor	Model	ATI Nano 43
	Channel	6-axis
	Force range	±36 N
	Torque range	±0.5 Nm
Measuring structure (Guide shaft)	Tilting range	±40°
	Rotating range	0–360°

4. Torque modeling through experimentation

4.1. Testbed for torque measurement

An experimental testbed is developed for the measurement of the torque generated between the PM-pole rotor and a single coil as shown in Fig. 7. The specification of this torque measurement apparatus is listed in Table 2. Unlike conventional torque measurements for single-axis actuators that have only one torque component, this testbed is able to measure three torque components for any rotor orientation in 3D workspace. A DC power (Topward 3303D) supplies current into the coil. A six-axis force/torque sensor is mounted on the rotor shaft to measure three torque components and three force components. The sensor has a measuring range of ±0.5 N m for torque components and ±36 N for force components. The rotor shaft can slide along the slot of the arc guide to incline a certain degree. The tilting angle is indicated by the dials on the arc guide. The guide shaft can also rotate about its own axis along with the rotor. The amount of rotation angle is indicated by the longitudinal rotation angle scale. The tilting and rotating motions determine the position of coil axis.

To reduce the measurement error, it is necessary to improve the concentricity of the rotor and the arc guide, i.e., make the rotor center coincide with the arc guide center. As illustrated in Fig. 8, the high-precision standard-sized blocks are utilized to support the rotor’s flat bottom surface to secure the rotor’s position. The screws beneath the rotor can be used to adjust the rotor’s position,

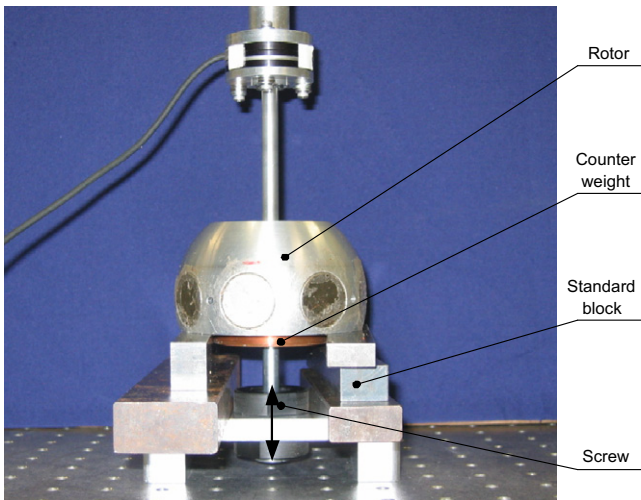


Fig. 8. Adjustment of the rotor position.

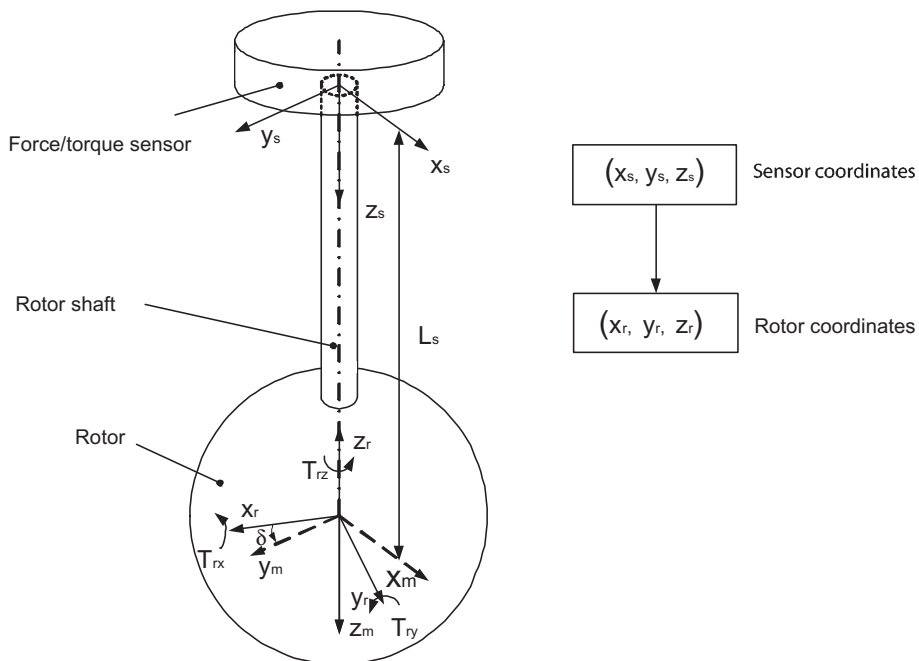


Fig. 9. Coordinate transformation of torque measurement.

and then be tightened to fix the rotor position. The standard blocks are removed after the adjustment to allow rotor motions. The counter weight on the rotor bottom is used to adjust the rotor's mass center.

4.2. Coordinate transformation from sensor to rotor

The raw data acquired from the six-axis force/torque sensor is based on the sensor coordinates as shown in Fig. 9. (x_s, y_s, z_s) represents the sensor coordinate system whereas (x_r, y_r, z_r) represents the rotor coordinate system. The measured data obtained from the sensor can be translated into the actual motor torque in rotor coordinate system by

$$\begin{bmatrix} T_{rx} \\ T_{ry} \\ T_{rz} \end{bmatrix} = \begin{bmatrix} -\sin \delta & \cos \delta & 0 \\ \cos \delta & \sin \delta & 0 \\ 0 & 0 & -1 \end{bmatrix} \left\{ \begin{bmatrix} T_{sx} \\ T_{sy} \\ T_{sz} \end{bmatrix} + \begin{bmatrix} F_{sy} \\ -F_{sx} \\ 0 \end{bmatrix} L_s \right\}, \quad (9)$$

where F_{sx}, F_{sy}, F_{sz} and T_{sx}, T_{sy}, T_{sz} are force and torque components based on the sensor coordinates, T_{rx}, T_{ry} and T_{rz} are torque components based on the rotor coordinates, L_s is the distance from the origin of the sensor coordinates to the rotor center. According to the apparatus assembly, there is a twist angle δ between the sensor coordinate system and the rotor coordinate system. In conducting the torque measurement, the distance from the coil to the rotor surface is kept close to zero. 3A current is supplied into the coil.

5. Experimental torque model

An analytical torque model is important for real-time motion control of electromagnetic actuators. Because the torque model developed in Eq. (7) is based on dihedral-shaped PM poles, it cannot be implemented to the spherical actuator with cylindrical PM poles. However, due to similar PM poles arrangement on the rotor surface, the magnetic field distribution trends surrounding the rotor and the corresponding actuator torque for both PM poles could be similar. Eight positive/negative peaks of the magnetic field should appear along the rotor equator, and the flux density decreases at points far from the equator. Thus, it is possible to formulate the torque output of the actuator with cylindrical-shaped PM poles through experimentation. In other words, by adjusting the terms in the analytical torque model according to the experimental measurement results, the torque model for the cylindrical-shaped PM rotor could be obtained.

Two approaches can possibly be used for the torque modeling. One method is to conduct measurement on the actual magnetic field of the rotor and to adjust the terms in the analytical magnetic field model to match the experimental result. The torque model can then be obtained by using Lorentz force law. This approach is not favorable because of accumulated errors from the measurement of magnetic flux density and the computation of torque integration. The alternative approach is to conduct experimental measurement on torque variation to formulate the torque model directly. This method can reduce the accumulated errors and simplify the computation. Therefore, it is employed in this study. Experimental measurement of the torque generated by a single coil is carried out with the torque measuring apparatus. Through comparing the analytical torque model with the experimental result, Eqs. (7) and (8) can be modified as torque model of cylindrical poles. There are mainly three modifications. First, according to experimental result, the frequency of torque variation in θ_p -direction increases 1.3 times with respect to the previous torque model. This is because the size of cylindrical-shaped magnet is very small in θ_p -direction, and thus the magnetic flux density drops down very fast. It is somehow like increasing the variation frequency in this direction. The rotor coordinates and the measurement

coordinates have the relationship of $\theta = \pi/2 - \theta_p$. Therefore, $\theta' = \pi/2 - 1.3\theta_p$. For the i th coil, it is $\theta'_i = \pi/2 - 1.3\theta_{pi}$. Second, ratios among three torque components can be observed from experimental result. It is found that torque components in x - and y -directions need to be multiplied approximately by 0.9. This is because the magnet takes more space in the rotor equator direction. Finally, the magnitude of the actuator torque can also be modified according to experimental result. By varying parameters of PM pole, the magnitude of the theoretical torque output can be adjusted. Therefore, dimensions of PM pole can be chosen to make the magnitude of theoretical result coincident with that of experimental result. For this prototype, the PM-pole dimensions are determined as $\alpha = 32^\circ$, $\beta = 32^\circ$, $R_b = 15$ mm and $R_r = 46.5$ mm. Therefore, the actuator torque output generated by a single coil is obtained as

$$\mathbf{T}_i = \begin{bmatrix} T_{xi} \\ T_{yi} \\ T_{zi} \end{bmatrix} = T_c \begin{bmatrix} 0.9g_x(\pi/2 - 1.3\theta_{pi}, \phi_i) \\ 0.9g_y(\pi/2 - 1.3\theta_{pi}, \phi_i) \\ g_z(\pi/2 - 1.3\theta_{pi}, \phi_i) \end{bmatrix} \mathbf{J}_i = T_c \mathbf{G}(\pi/2 - 1.3\theta_{pi}, \phi_i) \mathbf{J}_i. \quad (10)$$

The torque model for a full set of coils is thus

$$\mathbf{T} = T_c \begin{bmatrix} 0.9g_x(\pi/2 - 1.3\theta_{p1}, \phi_1) \dots 0.9g_x(\pi/2 - 1.3\theta_{pN}, \phi_N) \\ 0.9g_y(\pi/2 - 1.3\theta_{p1}, \phi_1) \dots 0.9g_y(\pi/2 - 1.3\theta_{pN}, \phi_N) \\ g_z(\pi/2 - 1.3\theta_{p1}, \phi_1) \dots g_z(\pi/2 - 1.3\theta_{pN}, \phi_N) \end{bmatrix} \begin{bmatrix} J_1 \\ J_2 \\ \vdots \\ J_N \end{bmatrix}.$$

These equations are valid within the range of $\theta_{pi} \in [-\pi/3, \pi/3]$ and $\phi_i \in [0, 2\pi]$. The normal distance d_a from the rotor surface to the top of the coil is approximately equal to zero. Magnets with $\mathbf{B}_{rem} = 1.29$ T (NdFeB 26 N-42H) are utilized for the PM rotor poles.

The experimental results and modified analytical model are transferred to stator coordinates and presented in Figs. 10–12. Figs. 10–12a show the variation of torque with respect to the stator angular parameters ϕ_s and θ_s . For ease of observation, only portions of the data are selected. The torque variation for certain fixed values of θ_s is illustrated in Figs. 10–12(b). It is found that the analytical model fits with the experimental measurement result

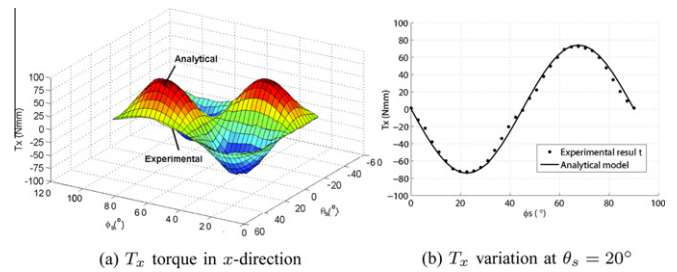


Fig. 10. Actuator torque T_x in x -direction of low-cost rotor.

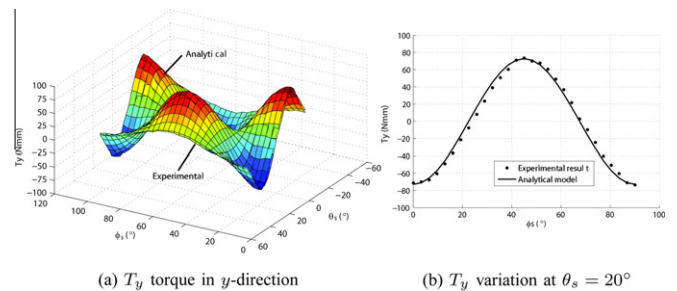


Fig. 11. Actuator torque T_y in y -direction of low-cost rotor.

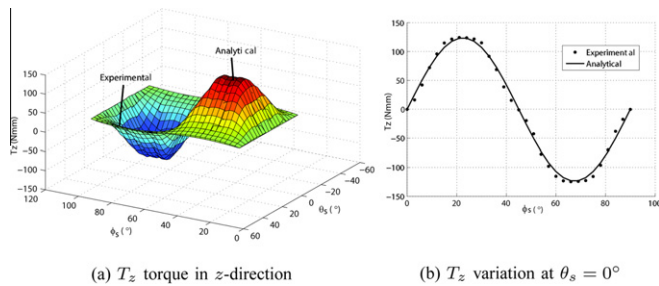


Fig. 12. Actuator torque T_z in z -direction of low-cost rotor.

well. The maximum difference between the theoretical model and experimental result is about 8%. The different may be decreased further by reducing the apparatus assembly and measurement errors. The robust control algorithm will be developed to reduce the effects of the model errors and the exogenous disturbances at the next stage.

6. Conclusion

A spherical actuator with cylindrical-shaped PM rotor poles is proposed in this study. Compared with the spherical actuator with dihedral-shaped PM rotor poles developed previously, the use of cylindrical PMs facilitates the fabrication of rotor poles and reduces the system cost greatly. Furthermore, due to the high density of rare-earth material, the employment of cylindrical PMs can decrease the rotor moment by more than 60%, which helps to achieve high dynamic performance of the spherical actuator. One challenging topic of the newly proposed PM spherical actuator design is to formulate the torque output, which is important for the real-time motion control of electromagnetic actuators. Because the torque modeling method that was used for spherical actuators with dihedral PM poles is no longer applicable, a hybrid torque modeling method that uses both experimental and analytical ways is proposed. A research prototype of the spherical actuator with cylindrical PM poles is developed, and a torque measurement apparatus is built up to conduct experiments on the prototype. The advantage of this measurement apparatus is that it can measure the variation of all three torque components with respect to the rotor orientations in a 3D workspace simultaneously. Due to the PM poles arrangement on rotor, the magnetic field distribution trend surrounding the rotor surface and thus the torque variation with respect to the angular parameters for both PM-pole designs are similar. Therefore, the parameters in the analytical torque model derived with Lorentz force law are modified to fit with the experimental results. The comparison of the modified analytical model and the experimental result shows that the difference between them is around 8% of the experimental result. The obtained analytical torque model can be used for the motion control of the PM spherical actuator together with robust control algorithm.

Acknowledgments

This work was supported by the National Nature Science Foundation for Distinguished Young Scholars of China (50825502), National Nature Science Foundation of China under the research

project 50975017, and the Fundamental Research Funds for the Central Universities.

References

- [1] Lu H, Zhu J, Lin Z, Guo Y. An inchworm mobile robot using electromagnetic linear actuator. *Mechatronics* 2008;19(7):1116–25.
- [2] Janaideh MA, Rakheja S, Su C-Y. Experimental characterization and modeling of rate-dependent hysteresis of a piezoceramic actuator. *Mechatronics* 2009;19(5):656–70.
- [3] Gomis-Bellmunt O, Galceran-Arellano S, Sudria'-Andreu A, Montesinos-Miracle D, Campanile LF. Linear electromagnetic actuator modeling for optimization of mechatronic and adaptronic systems. *Mechatronics* 2006;17(2):153–63.
- [4] Romano R, Tannuri EA. Modeling, control and experimental validation of a novel actuator based on shape memory alloys. *Mechatronics* 2009;19(7):1169–77.
- [5] Laithwaite ER. Design of spherical motors. *Electrical Times (London)* 1960;9:921–5.
- [6] F. Williams, E. Laithwaite, J.F. Eastham, Development and design of spherical induction motors, in: *Proceedings of the Institution of Electrical Engineers*, vol. 106, December 1959, pp. 471–184.
- [7] Davey K, Vachtsevanos G, Powers R. The analysis of fields and torques in spherical induction motors. *IEEE Transactions on Magnetics* 1987;23(1):273–82.
- [8] Lee KM, Kwan CK. Design concept development of a spherical stepper for robotic applications. *IEEE Transactions on Robotics and Automation* 1991;7(1):175–81.
- [9] Lee K-M, Meyouhas G, Blenis R. A machine-vision-based wrist sensor for direct measurement of three degrees-of-freedom orientation. *Mechatronics* 1993;3(5):571–87.
- [10] K.M. Lee, H. Son, J. Joni, Concept development and design of a spherical wheel motor (SWM), in: *Proceedings of the 2005 IEEE/ASME International Conference on Robotics and Automation*, July 2005, pp. 335–340.
- [11] Lee K-M, Ezenekwe DE, He T. Design and control of a spherical air-bearing system for multi-d.o.f. ball-joint-like actuators. *Mechatronics* 2002;13(2):175–94.
- [12] K.M. Lee, H. Son, Torque model for design and control of a spherical wheel motor, in: *Proceedings of the 2005 IEEE/ASME International Conference on Advanced Intelligent Mechatronics*, July 2005, pp. 335–340.
- [13] Lee KM, Roth RB, Zhou Z. Dynamic modeling and control of a ball-joint-like variable-reluctance spherical motor. *ASME Journal of Dynamic Systems, Measurement, and Control* 1996;118:29–40.
- [14] Wang J, Jewell GW, Howe D. Spherical actuators with multiple degrees-of-freedom. *IEEE Colloquium on Limited Motion Electrical Actuation Systems* 1998;1998/494:8/1–6.
- [15] Wang J, Jewell GW, Howe D. A novel spherical actuator with three degrees-of-freedom. *IEEE Transactions on Magnetics* 1998;34(june):2078–80.
- [16] Ackermann B, Steinbusch H, Vollmer T, Wang J, Jewell G, Howe D. A spherical permanent magnet actuator for a high-fidelity force-feedback joystick. *Mechatronics* 2004;14(3):327–39.
- [17] Chirikjian GS, Stein D. Kinematic design and commutation of a spherical stepper motor. *IEEE/ASME Transactions on Mechatronics* 1999;4(4):342–53.
- [18] Yang C, Baek YS. Design and control of the 3 degrees of freedom actuator by controlling the electromagnetic force. *IEEE Transactions on Magnetics* 1999;35(5):3607–9.
- [19] Kahlen K, Voss I, Priebe C, W De Doncker R. Torque control of a spherical machine with variable pole pitch. *IEEE Transactions on Power Electronics* 2004;19(6):1628–34.
- [20] Dehez B, Galary G, Raucent B. Development of a spherical induction motor with two degrees of freedom. *IEEE Transactions on Magnetics* 2006;42(8):2077–88.
- [21] Yan L, Chen I, Lim CK, Yang G, Lim W, Lee K. Design and analysis of a permanent magnet spherical actuator. *IEEE/ASME Transactions on Mechatronics* 2008;13(2):239–48.
- [22] Lequesne B. Permanent magnet linear motors for short strokes. *IEEE Transactions on Industrial Applications* 1996;32(1):161–8.
- [23] Kim W-J, Goldie JH, Gerver MJ, Kiley JE, Swenback JR. Extended-range linear magnetostrictive motor with double-sided three-phase stators. *IEEE Transactions on Industrial Applications* 2002;38(3):651–9.
- [24] Ustun O, Tuncay RN. Design, analysis, and control of a novel linear actuator. *IEEE Transactions on Industrial Applications* 2006;42(4):1007–13.
- [25] W Jansen J, Lierop CMMV, Lomonova EA, Van-denput AJA. Magnetically levitated planar actuator with moving magnets. *IEEE Transactions on Industrial Applications* 2008;44(4):1108–15.